The Detection and Classification of Microcalcifications in the Visibility-Enhanced Mammograms Obtained by using the Pixel Assignment-Based Spatial Filter

Mahmut HEKIM[1], Ayse AYDIN YURDUSEV[2], Canan ORAL[3]
[1]*Tokat Gaziosmanpasa University*, *Tokat*, *60150*, *Turkey*
[2,3]*Amasya University*, *Amasya*, *05100*, *Turkey*
ayse.yurdusev@amasya.edu.tr

***Abstract*—In this paper, we proposed a computer aided diagnosis (CAD) system which has the pixel assignment-based a spatial filter to enhance the visibility of microcalcifications in mammograms. This filter first sums the absolute values of the differences between the center pixel-of-interest and its 8-neighbors, and then assigns this summed value to that center pixel-of-interest. This process was repeated for each pixel of all images, and the contrast stretching was applied into all obtained images. Then, it was firstly detected by using different classifiers whether is absent/present of microcalcification in the obtained images, and the detected microcalcifications were classified as benign/malignant by using the same classifiers. In order to evaluate the effects of the proposed filter on the detection and classification successes, it was compared to widely used filters. In the implemented experiments, this comparison showed that the proposed filter provided higher contribution to the detection and classification successes than the others, and hence enhanced the visibility of microcalcifications in mammograms. Finally, it can be concluded that the CAD system with the proposed filter can contribute to the development of the state-of-art methodologies and can be used as a diagnostic decision support mechanism in the analysis of mammograms.**

***Index Terms*—biomedical image processing, cancer detection, computer aided diagnosis, mammography, spatial filters.**

I. INTRODUCTION

Breast cancer is a vital-threatening disease that can be metastasized to other parts of the body, and if it is not treated in after early diagnosis, it will result in death. The most effective way to treat a patient is only possible with early diagnosis. The earliest sign of breast cancer is calcifications which are the appearance of small calcium deposits on breast [1]. The calcifications are categorized into two groups depending on their size: macrocalcifications and microcalcifications where a microcalcification's length is less than 1 mm [2-3]. Various screening techniques such as Magnetic Resonance Imaging (MRI), Ultrasound, Computerized Tomography (CT) and Mammography are used for the detection of breast cancer. Among these techniques the mammography is the most common breast imaging technique which can help the diagnosis and treatment of breast cancer in early stages [1-4].

The detection of microcalcifications in mammograms is a challenging task since they have different erratic shapes such as blob, elliptical and circular, which make the detection process more complex and harder [5-6]. This nodular structure makes the detection of calcifications in mammograms difficult. Therefore, a number of nodules are overlooked by radiologists. The sensitivity of radiologists in the detection of microcalcification is about 70% - 90% [5]. Therefore, many researchers focused on computer-aided diagnosis (CAD) systems based on different algorithms in order to detect and classify the microcalcifications in mammograms. CAD systems which can be considered as a diagnostic tool for radiologists should focus on improving the diagnostic accuracy and consistency of image interpretations of radiologists [7-8]. There are many CAD systems designed for these purposes in the literature [5],[9-10],[17-18],[20]. However, many of these systems are based on thresholding algorithms and only use the pixel intensities of images, and therefore they need to enhance the visibility of microcalcifications to be successful of them. For this aim, special filters should be developed to enhance the visibility of microcalcifications. The main aim of these filters used in CAD systems is to improve the visibility of microcalcifications by suppressing the background tissues including fat, veins, glandular tissues or ducts. Therefore, many researchers have focused on providing a clear appearance of microcalcifications and suppressing the background [13-14],[15],[18]. Meersman et al. eliminated the background tissue using median filtering and enhanced the visibility of microcalcifications using a non-linear extremum filter. Then, the enhanced image was converted to binary sequences by using threshold techniques. They reached the total correct classification (TCC) ratio of 90% [21]. Catanzariti et al. suggested an algorithm that involves a set of Gabor filters for 16 mammograms. They cut off the normal breast area in the background, and then, applied to the Gabor filter set. The visibility-enhanced images were classified by using a three-layer feed-forward Artificial Neural Network (FFNN). The classifier reached the success ratios of 95% for both specificity and sensitivity [9]. Duarte et al., by means of thresholding and Top-hat transform on 236 mammographic Region of Interest (ROI) areas, reached to the segmentation performances of 54%, 31% and 10% in 5-pixel disc-shaped, 17-pixel disc-shaped and 7-pixel cross-shaped structural elements, respectively. Their classification performance for the segmentation of microcalcifications was 88.6% for this approach based on threshold and Top-hat transform [10]. Yasiran et al. used three edge detection masks to enhance the visibility of microcalcifications in mammograms taken from National Cancer Society Malaysia

Digital Object Identifier 10.4316/AECE.2019.04009

(NCSM) database. According to the evaluation of radiologists, Prewitt filter provided an Area the Under Curve (AUC) ratio of 0.79 under the Receiver Operating Characteristic (ROC) curve, which was more successful than Sobel and Laplacian of Gaussian (LoG) filters [11]. Kus and Karagoz reached the success ratios of 94% for both specificity and sensitivity on 57 mammograms by using an algorithm based on histogram stretching, unsharp masking and Support Vector Machines (SVM) [12]. These approaches containing filter integrated into CAD systems reached successful results, which are based on the segmentation of microcalcifications in mammograms. However, they did not take into account the microcalcifications in different sizes and shapes on the mammogram. Since microcalcifications are nodular in structure, the success of CAD system depends on filtering methods or the used other techniques. Therefore, we proposed a novel spatial filter enhancing the visibility of microcalcificaitons in mammograms so that they could be detected and classified by using the classifiers at higher success rates. This filter first sums the absolute values of the differences between the center pixel-of-interest and its 8-neighbors, and then assigns this summed value to that center pixel-of-interest. This process was repeated for each pixel of all images, and the contrast stretching was applied into all obtained images. The contribution of the proposed filter to the success of classifiers in the detection and classification of microcalcifications in mammograms was investigated. For this aim, we designed a CAD system using this filter to improve the diagnostic performance of radiologists. For this aim, the proposed filter was applied to mammographic ROIs, and these filtered-mammographic ROIs were stretched by using contrast stretching. The feature vectors were extracted from the contrast stretched-mammographic ROIs by means of statistical parameters which are mean, standard deviation, entropy, energy, skewness and kurtosis. Then, the extracted feature vectors were used as the inputs of SVM, Multilayer Perceptron Neural Network (MLPNN) and Linear Discriminant Analysis (LDA) based classifiers in order to not only detect the microcalcifications in mammograms as present/absent and both also classify them as benign/malignant, respectively. The same classification experiments were reimplemented for widely used Top-hat, Gabor, Laplacian and Gaussian High Pass (GHP) standard filters to compare with the proposed filter, and then the obtained results were evaluated by using the ROC analysis. Fig. 1 shows the overview of the proposed approach which consists of the two following stages: in first, the detection of microcalcifications in mammograms as absent/present, and in second, the classification of the detected microcalcifications as benign/malignant.

The proposed CAD algorithm can be summarized with the following steps:

1. Prepare ROIs from the database, and
   if microcalcification is known,
   crop by chain code
   else crop at the center of the breast.
2. Prepare ROIs by using each following filtering method, separately.
   a. Keep ROI as Original
   b. Laplacian Filter with kernel [0 -1 0, -1 4 -1, 0 -1 0]
   c. Gabor Filter
   d. GHP filter
   e. Top-hat Filter
   f. Proposed Filter
3. Apply contrast stretching to all filtered ROIs
4. Extract statistical feature sets and normalize them
5. Classify all mammograms as present/absent of microcalcification by using SVM / LDA / MLPNN.
6. Classify the mammograms with microcalcifications as benign and malignant by using SVM / LDA / MLPNN.

This paper is organized as follows. "Material and Method" section describes the used materials and methods for the detection and classification of microcalcifications in mammogram ROIs. "Results" section presents the obtained classification results and the performance analysis, in detail. "Discussion" section puts forward discussion, evaluation and concluding remarks.

II. Material and Method

In this study, 219 mammograms were taken from the Digital Database for Screening Mammography (DDSM) were divided into two groups: 124 normal (the absence of microcalcification) and 95 abnormal (the presence of microcalcification). The ROIs taken from mammograms were prepared for normal and abnormal cases (benign and malignant microcalcifications). For normal cases, breast tissues were unsystematically cropped from mammograms. However, for abnormal cases, mammograms were cropped by chain code which is a labeling technique that gives the coordinate of the start pixel and draws the edge of the area by using the numbers [22]. The size of each ROI was selected as 512×512 pixels. More detail is on the webpage [23].

A. The pixel assignment-based spatial filter

Many filters used in CAD-based analyses of mammograms have been used with together commonly used image processing methods to further improve the quality of images [6],[10-11],[13-14],[17],[24-25]. While some filters denoise various noise types such as quantum or artifact noise from the images [10-11], some of them enhance the visibility of particular specifications [13-14]. In this study, we focused on a special filter for concretizing and enhancing the visibility of microcalcifications in the ROIs instead of denoising various noise types. The visibility enhancement of microcalcifications can be possible with tissue analysis, in detail. The microcalcifications have the structures with gradually increasing intensities from the outer circumference to the center, in general. Therefore, this filter proposed in the study first sums the absolute values of differences between each center pixel and its 8-neighbors and assigns this sum value to that center pixel. Thereby, the filter becomes independent of background intensity values.

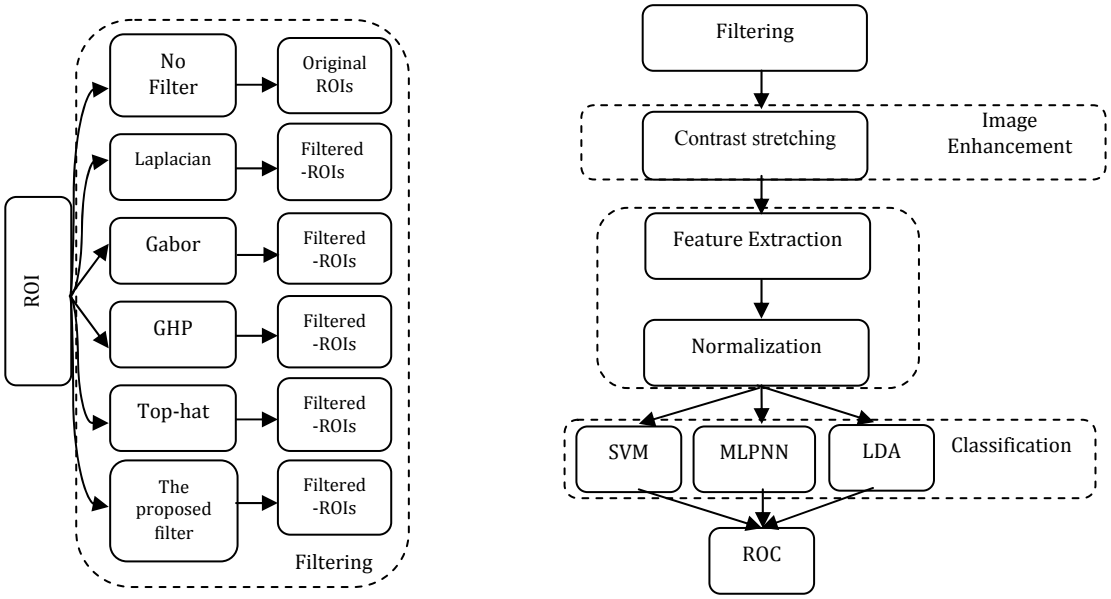

Figure 1. The block diagram of the proposed approach

The formula of the proposed spatial filter is described as

$$\begin{aligned} K(x,y) = & |f(x-1,y-1)-f(x,y)|+|f(x-1,y)-f(x,y)| \\ & +|f(x-1,y+1)-f(x,y)|+|f(x,y-1)-f(x,y)| \\ & +|f(x,y+1)-f(x,y)|+|f(x+1,y-1)-f(x,y)| \\ & +|f(x+1,y)-f(x,y)|+|f(x+1,y+1)-f(x,y)| \end{aligned} \quad (1)$$

$$K(x,y)=\sum_{i=-1}^{1}\sum_{j=-1}^{1}\left|f(x+i,y+j)-f(x,y)\right|$$

where, $f(x,y)$ is the center pixel of the original image size of MxN, and $K(x,y)$ is the calculated value of the center pixel. In order to generate a completely filtered image, the formulas were applied for the determination of the calculated values of all pixels of the image (i.e., for $x=1,2,3,\ldots,M-1$ and $y=1,2,3,\ldots,N-1$).

The algorithm of the proposed filter is presented below:

1. Get ROI size of MxN
2. Apply symmetric padding to ROI with 10 pixels for each edge
3. for x=2:M+9
   for y=2:N+9
   Calculate center pixel $K(x,y)$ to be assigned for center pixel-of-interest $f(x,y)$ by using Equation 1
   end
   end
4. Assign the calculated center pixel $K(x,y)$ value to center pixel-of-interest $f(x,y)$ value
5. Repeat Step 3 and 4 for all pixels of the image
6. Crop the symmetric padded-ROI back into the size of MxN

The elapsed time of the proposed filter was 50.22 ms on average for each ROI. This elapsed time usage is acceptable in point of view of applicable processing burden for a diagnostic CAD system.

In the implemented experiments, we investigated the contribution of the proposed filter to the performance of classifiers in the detection and classification of microcalcifications in mammograms. To illustrate the contribution of the proposed filter, we compared with widely used other Top-hat, Gabor, Laplacian and GHP standard filters. An overview of the used filters for comparison with the proposed spatial filter as follows:

Top-hat filtering: it is a type of morphological filters in order to emphasize different shapes on an image, which is also known as Top-hat transform. This filter focuses on high-intensity values in the image. It firstly opens the images by using the opening operation, and then subtracts the opened images from the original ones. The simplest and most effective way of this filtering that the images are convoluted by a disk shape kernel, and in this way, clearer disk shapes in the image are created. Although the shape, brightness and distribution of microcalcifications are different one from each other, in general they are very small and have a roughly round shape. Therefore, the disk shape kernel was chosen for the convolution since microcalcifications are round shaped. The radius of the kernel was chosen as 10 pixels because of that the dimension of a small microcalcification is about 10 pixels (0.4mm) for 40um resolution.

Gabor filter: it is a bandpass filter that multiplies a complex sinusoidal signal by a Gaussian envelope [26]. The simplified representation of a two-dimensional Gabor function (the bandwidth is 1 octave; the phase shift is zero; and the kernel is in the center) is given as

$$g(x,y)=e^{-\frac{x'^2+\gamma^2y'^2}{2\sigma^2}}\cos(2\pi\frac{x'}{y}) \quad (2)$$

$$x'=(x)\cos\Theta-(y)\sin\Theta \quad (3)$$

$$y'=(y)\cos\Theta+(x)\sin\Theta \quad (4)$$

where, x and y represent the position of the pixel, γ is the spatial aspect ratio which is the ratio of minor-axis to major-axis of Gaussian distribution. σ is the standard deviation of Gaussian distribution and it is related to wavelength (σ=0.56λ). Θ is the orientation of the Gabor filter range between 0-360 degrees [27–29]. In this study, considering the small size, elliptical shape and eccentricity of microcalcification, the parameters were selected as 3 pixel/cycle, 90 degrees and 0.5 for wavelength, orientation, and spatial aspect ratio, respectively.

Laplacian filter: it is used for the improvement of the details of the image, which is based on second-order derivatives. The simple form of a two-dimensional Laplacian operator is given as follows [30].

$$\Delta^2 f=\frac{\partial^2 f}{\partial x^2}+\frac{\partial^2 f}{\partial y^2} \quad (5)$$

$$\Delta^2 f(x,y) = f(x-1,y) + f(x+1,y) + f(x,y-1) + f(x,y+1) - 4f(x,y) \quad (6)$$

where, *f(x,y)* is an output pixel on the coordinate (*x,y)*. In this study, we used a straightforward and well-known Laplacian kernel given in Eq. 6.

The Gaussian high pass (GHP) filter: it is a type of high pass filter that passes frequencies higher than cut-off frequency and suppresses lower ones in the frequency domain. Hence, a high pass filter improves the visibility of details and denotes the edges of the images. The GHP filter has the cut-off frequency with Gaussian distribution which provides a smooth transition from low frequencies to higher ones, thus it eliminates ringing effects. The mathematical formulas of GHP filter are given by

$$H(u,v) = 1 - e^{-\frac{D^2(u,v)}{2D_0^2}} \quad (7)$$

$$D(u,v) = \sqrt{\left(u - \frac{M}{2}\right)^2 - \left(v - \frac{N}{2}\right)^2} \quad (8)$$

where u and v are the coordinates of a pixel in the frequency domain, $M \times N$ is the size of the image and D_0 is cut-off frequency [31]. In this study, the size of the ROIs and cut-off frequency were selected as 512×512 pixels and 15 Hz, respectively. This cut-off frequency providing the best visibility of microcalcifications for the used dataset was determined by investigating its optimum value in ROIs.

The images obtained by using Laplacian and Gabor filters in the implemented experiments had narrow dynamic ranges, so the visual examination of the effects of the filters in the images was extremely difficult. The implementation of contrast stretching on the filtered images with narrow dynamic ranges was necessary to equalize the visibility of microcalcifications in the images. Therefore, the contrast stretching was applied to all filtered and original images used in the study to ensure that the dynamic range was equalized for all images, although it was not required for other filtered images. This step provided a fair start for the feature extraction stage. Fig. 2 (a), (b) and (c) show an original full-size ROI of 512×512 pixels, the filtered-ROI obtained from ROI using the proposed filter and the filtered-contrast stretched-ROI obtained from the filtered-ROI using contrast stretching, respectively. As seen in Fig. 2 (a), the microcalcifications on original ROI were hardly noticeable to the naked eye. In (b) and (c), the edges of microcalcifications on both filtered-ROIs became visible compared to their originals since the backgrounds of both were suppressed by using the proposed filter, namely the microcalcifications in the filtered-ROIs came to the fore in proportion to their originals. However, as seen in (c), the visibility of microcalcifications in the filtered-ROI was enhanced by using contrast stretching that expands the dynamic range of the image. In consequence, the proposed filter resulted in further improvement on the visibility of the clusters of microcalcifications, allowing a detailed study of their physical properties such as shape, size and distribution.

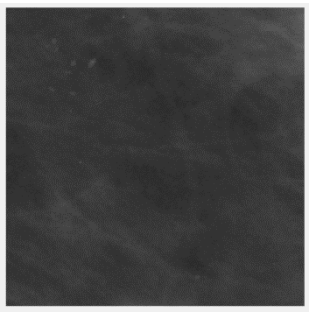

a) The original ROI

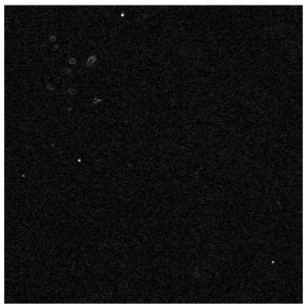

b) The filtered-ROI

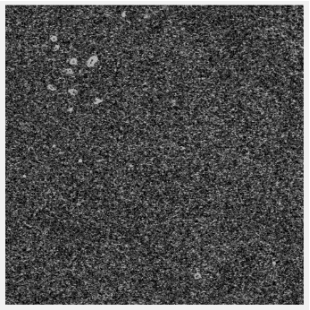

c) The filtered-contrast stretched-ROI

Figure 2. The images filtered by the proposed filter

To illustrate the contribution of the proposed filter for the visibility enhancement of microcalcifications, we also applied Top-hat Laplace, Gabor and GHP filters, after that, contrast stretching to the filtered images. Figure 3 shows the filtered-contrast stretched-ROIs which were obtained by applying contrast stretching to the filtered-ROIs produced by using Top-hat, Gabor, Laplacian and GHP filters.

Figure 3 (a) and (b) show that the used filters were ineffective in terms of the improvement of the visibility of microcalcifications and the suppression of background noises. In Figure 3 (c) and (d), the visibility of microcalcifications was improved by the filters used for comparison and contrast stretching, but background tissues could not be eliminated, completely.

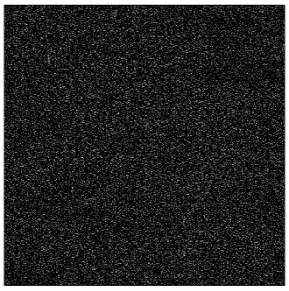

a) Laplacian filtered-contrast stretched-ROI

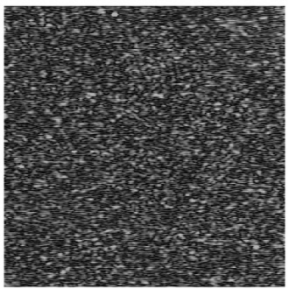

b) Gabor filtered-contrast stretched-ROI

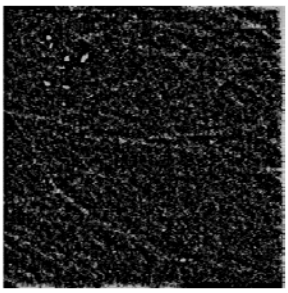

c) GHP filtered-contrast stretched-ROI

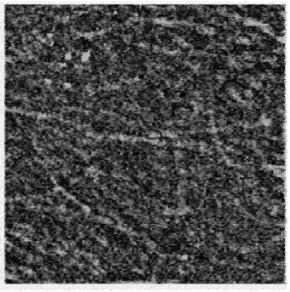

d) Top-hat filtered-contrast stretched-ROI

Figure 3. The images of filtered by other filters

B. Feature Extraction

The aim of the feature extraction is to transform the original image into the dataset with a reduced number of variables that contains the most discriminatory information. This procedure reduces the data dimensionality, remove redundant or irrelevant information, and convert it a form more appropriate for subsequent classification. In order to improve the classification performance and reach achievable classification processing speed, a more stable representation should be provided by reducing the bandwidth of the input data to classifiers [32]. The feature extraction parameters used in this study were selected from widely used data reduction procedures that are very effective in identifying microcalcifications in literature, which are mean, standard deviation, entropy, energy, skewness and kurtosis [32-33]. Table I shows the parameters used for extracting the statistical features of the images.

TABLE I. THE PARAMETERS USED FOR EXTRACTING THE STATISTICAL FEATURES OF THE IMAGES

Parameters	Formulas
Mean (m)	$m = \sum_{i=0}^{L-1} i p_i$
Standard Deviation (σ)	$\sigma = \sqrt{\sum_{i=0}^{L-1} (i-m)^2 p_i}$
Entropy (I)	$I = -\sum_{i=0}^{L-1} p_i \log_2 p_i$
Energy (E)	$E = \sum_{i=0}^{L-1} p_i^2$
Skewness (S)	$S = \frac{1}{\sigma^3} \sum_{i=0}^{L-1} (i-m)^3 p_i$
Kurtosis (K)	$K = \frac{1}{\sigma^4} \sum_{i=0}^{L-1} (i-m)^4 p_i$

where p_i is a normalized cumulative histogram (p_i=h_i/N), N is the total pixel number, h_i is gray-level histogram (i=*1*, *2*,*3*,...*L-1*), and L is the number of gray-level of the image.

C. Classification

In CAD systems, decision-making mechanisms can be produced with unsupervised or supervised algorithms. One of the best known and widely used unsupervised algorithms is the k-means clustering algorithm [34-35]. There are studies on k-means clustering and depending approaches in the literature [34–36]. However, in this study we choose to use classification algorithms. Some of classification algorithms can classify multi-relational dataset [37]. Nevertheless, we prefer to use traditional classification algorithms that suit well with our problem of interest.

In this study, three different classifiers were selected from both linear and non-linear classifiers since the characterization of the extracted feature spaces was unspecified. The classifiers based on SVM, MLPNN and LDA used in the study are represented below in detail.

1) Support Vector Machine (SVM)

The SVM is a discriminative classifier defined by a separating hyperplane. In this technique, a given dataset is transformed to the hyperplane, and it is divided into the groups according to the hyperplane. If the hyperplane cannot separate the dataset into classes, SVM creates another hyperplane by using the kernel and moves the dataset to the new hyperplane. Then, it chooses the best separation line that has a maximum distance between groups. This maximum distance is called optimal separation hyperplane and the nearest data to the margin are called as support vectors [38]. The SVM classifier function is defined by

$$\mathrm{f}_{\mathrm{SVM}}(\mathrm{x}) = \sum_{k=1}^{K} K(x, s_k) + b \tag{9}$$

$$K(x, s_k) = \phi^T(x)\phi(s_k) \tag{10}$$

where b is bias, ϕ is nonlinear mapping function, x is the input vector, s_k is the support vector and K is the kernel function.

Typically, three types of kernels are used for optimal SVM: linear, polynomial and radial basis function (RBF)

kernels. In general, while the linear kernel is suitable for linearly separable datasets, polynomial and RBF kernels are suitable for non-linearly separable datasets. As parameters p and σ are obtained during the process, the kernels are formulated by [39].

$$K(x_i, x_j)_{Lin} = x_i^T x_j \tag{11}$$

$$K(x_i, x_j)_{Poly} = (x_i^T x_j + 1)^p \tag{12}$$

$$K(x_i, x_j)_{RBF} = e^{\gamma \|x_i - x_j\|^2} \tag{13}$$

where $\gamma = (2\sigma^2)^{-1}$

In this study, we used the SVM classifier with RBF kernel since it is more suitable for non-linearly separable data than the others. Also, the value of σ parameter was determined 2.8 in this way of trial-and-error.

2) Multilayer Perceptron Neural Network (MLPNN)

The Multilayer Perceptron Neural Network (MLPNN) classifier is one of the most preferable feed-forward neural network algorithms because it has the advantages of fast operation algorithm and lack of the complexity of implementation, and so it does not require a large amount of training data [39-40]. The MLPNN consists of at least three layers which are an input, a hidden and an output layer. The input layer introduces the input data, the hidden layer processes and transmits the input information to the output layer, and the output layer proposes the outcomes. The insufficient or excessive number of neurons in the hidden layer can cause miss-training or overfitting problems, hence the number of neurons is important. However, there is no specific method or formula to find the number of exactly required neurons. The number of neurons in the hidden layer is mostly determined by trial-and-error [40]. In this study, a MLPNN with a single hidden layer of 10 neurons was used for the classification experiments because it reached to the most successful results in terms of a good generalization.

Each neuron j in the hidden layer, sums the multiplication of its inputs (x_i) and their respective connection weights (w_{ij}). The output of each neuron (y_j) is described as follows:

$$y_j = f(\sum w_{ij} x_i) \tag{14}$$

where, f is the activation function using the weighted summations of the inputs. An activation function can be as simple threshold, sigmoid, or hyperbolic tangent function. In this study, a hyperbolic tangent function was used as the activation function.

The success of each activation function is evaluated by the sum of squared differences between the desired and the actual values of the output neurons. This sum E is defined as follows [41]:

$$E = \frac{1}{2}\sum_j (y_{dj} - y_j)^2 \tag{15}$$

where y_{dj} is the desired value of output neuron j and y_j is the actual output value of that neuron j. Each weight w_{ij} of a neuron is readjusted to minimize error ratio E [41]. The adjustment of error ratio E is widely realized by the backpropagation algorithm. The backpropagation algorithm has a couple of variations to determine the optimum weights. Therefore, in this study, we used the backpropagation algorithm supported by the Levenberg–Marquardt (LM) algorithm [40-41]

3) Linear Discriminant Analysis (LDA)

Linear Discriminant Analysis (LDA) method is widely used for both classification and dimensionality reduction. As a classifier method, LDA tries to find the best discriminative vectors in order to maximize the separability of classes by the way of separating the samples from two or more classes [42–44]. This process can be achieved in three steps: in the first step, the calculation of the separability between different classes (i.e. the distance between the mean of different classes) also called as the between-class scatter matrix; in second, the calculation of the distance between the mean and sample of each class, which is called the within-class scatter matrix; and in third, the construction of the lower dimensional space which maximizes the between-class variance and minimizes the within-class variance. The mathematical expressions of these three steps are below defined by equations 16, 17 and 18, respectively [42–44]. The mathematical expressions of the between-class and the within-class scatter matrices is given by

$$S_b = \sum_{i=1}^{c} N_i (\mu_i - \mu)(\mu_i - \mu)^T \tag{16}$$

$$S_w = \sum_{i=1}^{c} \sum_{x_k \in x_i} (x_k - \mu_i)(x_k - \mu_i)^T \tag{17}$$

where, c is the number of classes, N_i is the number of samples in ith class X_i, μ_i is the mean of ith class X_i, μ is the mean of all X_i classes, and x_k is the samples belonging to ith class.

After calculating the S_b and S_w, the transformation matrix (or the projection matrix), w_{LDA} can be calculated as in Eq. 18, which is called Fisher's criterion.

$$w_{LDA} = \arg\max_w \frac{w^T S_b w}{w^T S_w w} = [w_1, w_2, w_3 ... w_m] \tag{18}$$

This formula can be rewritten as in Eq. 19.

$$S_b w_i = \lambda_i S_w w_i \tag{19}$$

where, λ_i and w_i denotes the eigenvalues and eigenvectors of the transformation matrix (w_{LDA}), respectively. The LDA purposes to find the maximum ratio of the determinant of S_b to the determinant of S_w. Therefore, the final solution can be obtained by calculating the eigenvalues (λ_i) of λ and eigenvectors (w_i) of w, where, $\{w_i \mid i=1,2,...,m\}$ and $\{\lambda_i \mid i=1,2,...,m\}$, and m is the upper limit of class [45].

D. Validity criterion

The ROC analysis was generally used for evaluating the classification experiments. The ROC curve of the analysis demonstrates the sensitivity and specificity ratios. In order to draw this curve, four statistical measures, which are TP, TN, FP and FN, have to be determined in the result of the implemented classification. True Positive (TP) is the number of true positive decisions, True Negative (TN) is the number of true negative decisions, False Positive (FP) is the number of false positive decisions, and False Negative (FN) is the number of false negative decisions. *Sensitivity* is the ratio of the number of TP decisions to the number of actual positive cases (TP+FN). *Specificity* is the ratio of the number of TN decisions to the number of actual negative cases (TN+FP). Total correct classification (TCC) is the ratio of the number of correctly classified decisions (TN+TP) to the number of all cases (TN+FN+TP+FP) [46].

$$TCC = \frac{TP + TN}{TP + TN + FP + FN} \quad (20)$$

$$Sensitivity = \frac{TP}{TP + FN} \quad (21)$$

$$Specificity = \frac{TN}{TN + FP} \quad (22)$$

III. Results and Discussion

In this study, all experiments were implemented in MATLAB 2016a computation tool. All ROIs were also filtered by using both the proposed filter and the others to compare their performances, and the filtered ROIs and their originals were stretched by using contrast stretching in order to ensure fairness in the comparison of the contribution of the proposed filter. Then, the feature vectors were computed by well-known common statistical parameters which are mean, standard deviation, entropy, energy, skewness and kurtosis for both the filtered-contrast stretched-ROIs and the original-contrast stretched-ROIs. In order to reduce the computational burden and increase the classification accuracy, these feature vectors for 219 cases were normalized by

$$x_n = \frac{x_i}{\max|x_i|} \quad (23)$$

where, x_i is ith feature vector, $max|x_i|$ is the absolute maximum value of x_ith feature vector and x_n is normalized value of ith feature vector. The normalized feature vectors were used as the inputs of SVM and LDA linear classifiers and MLPNN nonlinear classifier for both the detection of microcalcifications in mammograms as absent/present and also the classification of microcalcifications as either benign or malignant.

To validate the used classifiers in both experiments, the data consisting of 219 mammograms were divided into two groups in the ratios of 50% according to 2-fold cross-validation: training dataset and testing dataset. 2-fold cross-validation is the simplest type of k-fold cross-validation, which is also called the holdout method. In this method, for each fold, data points are randomly assigned to two sets d_0 and d_1 so that both sets are of equal size. After that, the classifier is trained on d_0 and tested on d_1, followed by training on d_1 and testing on d_0. This provides an advantage for a large amount of training and testing sets, and each data point is used for both training and validation on each fold. Then the algorithm evaluates the classification error and decides the best training and testing groups [47].

We implemented two different experiments into: (1) the detection of microcalcifications in mammograms as absent or present, and (2) the classification of microcalcifications as benign or malignant, where a total of 95 mammograms were retrieved from the DDSM database, and cropped with chain codes at *512×512* pixels. Table II and III show the used training and testing datasets constructed for both experiments according to 2-fold cross-validation. The ROC analysis of the experiments implemented for the detection of the present/absent of microcalcifications is shown in Figure 4. The ROC analysis for the classification of the original contrast-stretched-ROIs had a good decision ratio. Sensitivity and specificity were between 58% - 62.5% and 99.9 - 100% for all classifiers, respectively. According to this scenario, the TCC ratio for the detection of the absence of microcalcification was 100%. However, the TCC ratio for the detection of the presence of microcalcifications was just about 60%.

Table II. The Used Training and Testing Datasets for the Detection of Microcalcifications

Mammograms	Training	Testing	Total
with microcalcifications	47	48	95
without microcalcifications	62	62	124
Total mammograms	109	110	219

Table III. The Used Training and Testing Datasets for the Classification of Microcalcifications

Microcalcification	Training	Test	Total
Benign	18	18	36
Malignant	29	30	59
Total	47	48	95

The ROC analysis for the Laplacian filtered-contrast stretched-ROIs has a similar result to the ROC analysis for the original contrast stretched-ROIs. Sensitivity and specificity were 66.6 - 70.1% and 99.9 - 100%, respectively. At this point, the used classifier models for the Laplacian filtered-contrast stretched-ROIs and the original-contrast stretched-ROIs could not generally determine the presence of microcalcifications. The Gabor and GHP filtered-contrast stretched-ROIs had insufficient generalization, and thus the classification results were near to randomness. The achievement of the classification considerably decreased due to the microcalcifications and the background noise in the images obtained by using these filters. The ROC analysis for the Top-hat and the proposed approach filtered-contrast stretched-ROIs demonstrated better classification performances. For the Top-hat filtered-contrast stretched ROIs, sensitivity-specificity ratios were 75% - 100%, 83% - 97%, and 88% - 87% for LDA, MLPNN and SVM classifiers, and their TCC ratios were 89.09%, 90.9% and 87.28%, respectively. The classification evaluation ratios for the proposed approach filtered-contrast stretched-ROIs had higher sensitivity-specificity decisions which were 81% - 98%, 83% - 94%, and 91% - 89% for LDA, MLPNN and SVM classifiers, respectively. The LDA classifier reached to the highest TCC ratios among them. Therefore, it was selected for comparison with previous studies, and this comparison is presented in Table IV.

Table IV. The Studies about Microcalcification Detection

Authors	Method	Sens.	Spec.	TCC
Meersman et. al [21]	Non-Linear Extremum Filter	--	--	90
Catanzariti et. al [9]	Gabor Filter Set	95	95	--
Duarte et. al [10]	Morphological Filter	--	--	88.6
Kuş et. al [12]	Unsharp Masking	94	--	--
Hekim et. al	Proposed Filter	98.4	81.3	90.9

As seen in Table IV, the proposed filter had higher sensitivity and TCC values than previous studies.

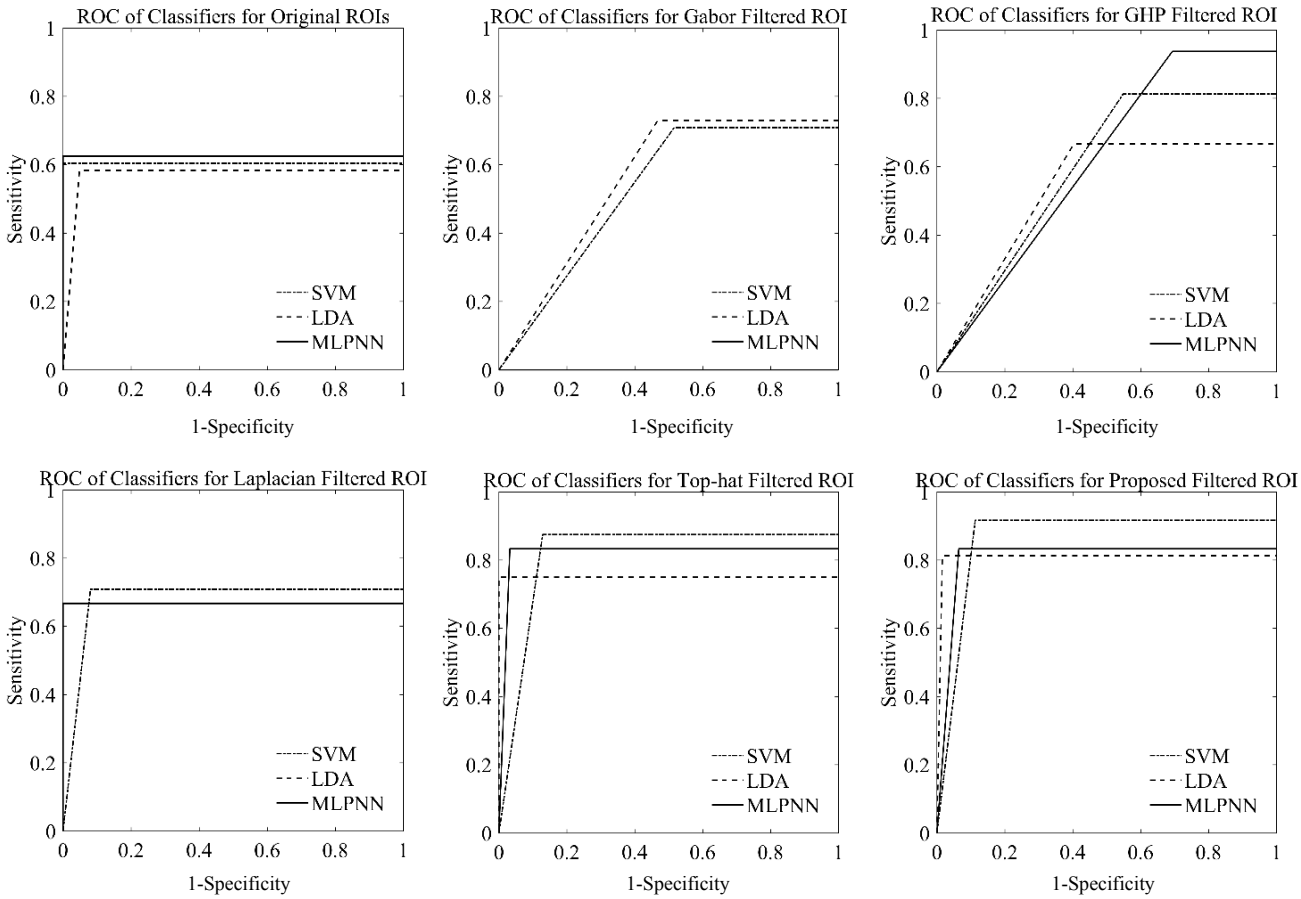

Figure 4. The ROC analysis for the detection of present/absent of microcalcifications

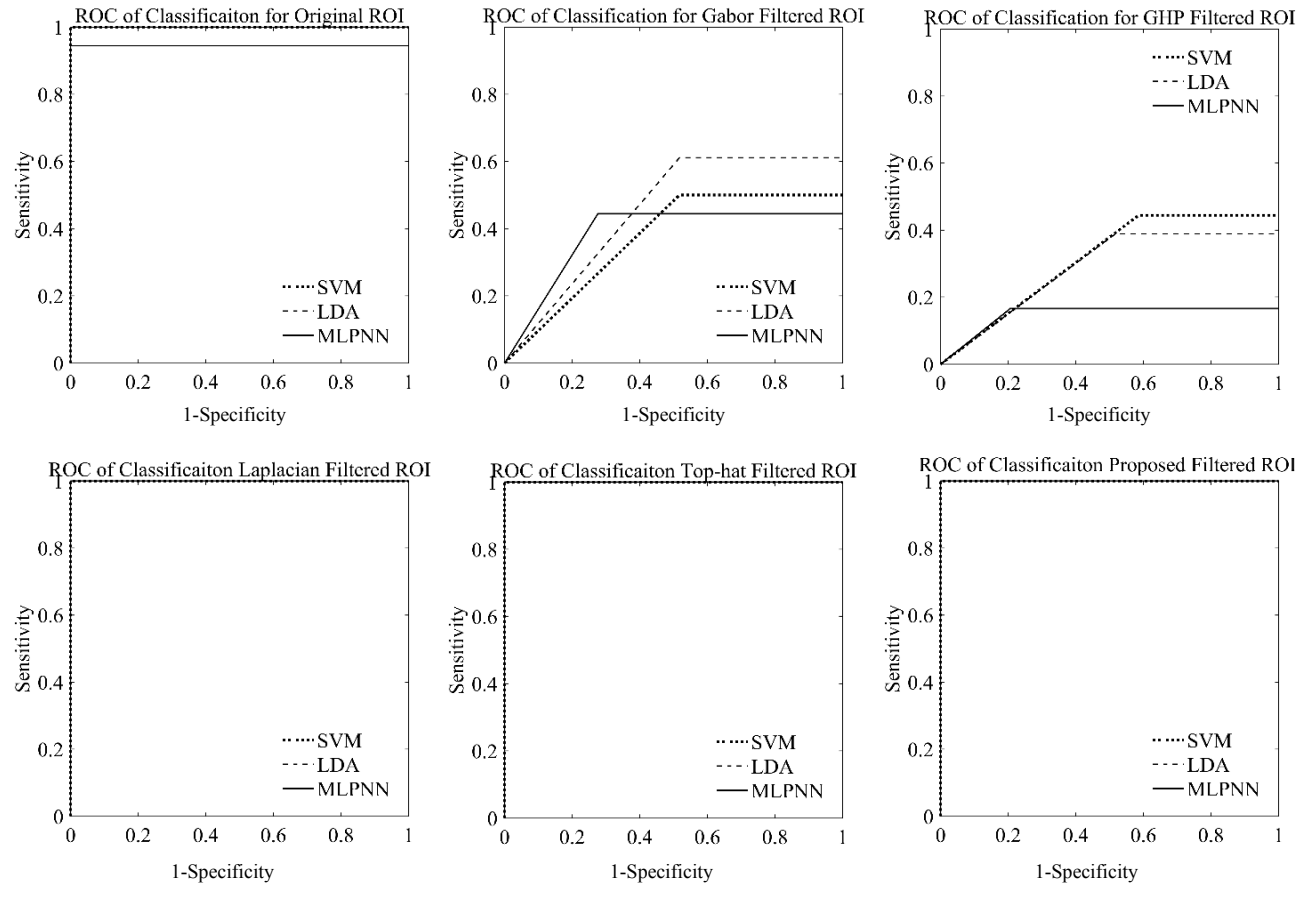

Figure 5. The ROC analysis for the classification of microcalcifications as benign and malignant

The TCC ratios for the proposed approach filtered-contrast stretched-ROIs were 90.9% for LDA and MLPNN classifiers and 90% for the SVM classifier.

The ROC analysis results of the classification of microcalcifications in mammograms are illustrated in Figure 5. The sensitivity and the specificity ratios for the classification of the original-contrast stretched-ROIs were 100% for both SVM and LDA classifiers, while the MLPNN classifier had the sensitivity of 95% and the specificity of 100%. The ROC analysis of the classifiers for the Gabor and GHP filtered-contrast stretched-ROIs showed exceptionally low classification accuracy. The TCC ratio for the Gabor filtered-contrast stretched-ROIs was around 50%, which is near to randomness. There was an inverse correlation between target classes and outcome classes, therefore the classifiers tended to label classes inverse such as label a positive case as negative and vice-versa for the GHP filtered-contrast stretched-ROIs. However, the best results of classification were obtained when using the Laplacian filter, Top-hat filter and the proposed filter. The ROC curves of the classification experiments implemented for Laplacian filter, Top-hat filter and the proposed filter were 100% for sensitivity, specificity and TCC of all classifiers.

IV. Conclusion

In this paper, a novel spatial filter was introduced for enhancing the visibility of microcalcifications in mammograms and suppressing the background tissues such as glandular tissues and fat tissues so that microcalcifications could be detected and classified at higher success ratios. In addition, we proposed a CAD system designed for testing the contribution of the proposed filter to the detection and classification. The proposed filter, a part of this CAD system, assigns the sum of the absolute values of the differences between the pixel-of-interest and its 8-neighbors to that pixel-of-interest. Some of the histogram ranges of the filtered images were very narrow such as images filtered by Laplacian filter and others histogram ranges were wider. Narrow histogram range could lead to miscalculation of the feature vectors. Thus, the contrast stretching was applied to the filtered images and the original images to ensure the conformity all images the feature vectors are calculated by using widely used statistical parameters which were mean, standard deviation, entropy, energy, skewness and kurtosis and these feature vectors were used as the inputs of SVM, MLPNN and LDA classifiers in order to detect microcalcifications in mammograms and classify them as malignant and benign. To illustrate the contribution of the proposed filter to the detection and classification of microcalcifications in mammograms, it was compared with Top-hat, Gabor, Laplacian and Gauss high pass filters widely used in the literature. The SVM and LDA classifiers for the filtered mammograms obtained by using the proposed filter reached to the best percentages in the detection of microcalcifications in mammograms. The results of the SVM and LDA classifiers for these filtered mammograms by the proposed filter were 2.73 and 1.8 percentages higher than the closest filter success, respectively. In addition, the proposed filter provided an improvement of 5.45, 7.27 and 11.82 percentages in the classification performance of original mammograms for MLPNN, SVM and LDA classifiers, respectively. In experiment 2, the proposed filter was labeled correctly the type of microcalcifications as benign or malignant with the rate of 100% sensitivity, specificity and TCC values by all classifiers. Experimental results showed that the proposed filter provided promising results in the performance of the classification since it could enhance the visibility of microcalcifications while suppressing the background noises and tissues. Despite the designed CAD system which has this simple spatial filter was not an advanced algorithm including morphological operations, threshold techniques, cascade or/and hybrid filtering, it reached to remarkable TCC ratios in the detection of microcalcifications in mammograms as absent/present and the classification of these detected microcalcifications as benign/malignant. As a result, it can be conclusively stated that the proposed filter provides an important contribution to the detection and classification of microcalcifications in mammograms.

In future works, the proposed filter can be used for an advanced CAD system for the detection and classification of microcalcifications in mammograms. Some further image processing algorithms, such as thresholding techniques and morphological operations, may improve the classification results gradually.

References

[1] R. Kumari, S. Venkatesh. "Breast cancer imaging techniques - A comparative study", Materials Today: Proceedings, vol. 5, no. 4, pp. 10792–10796, 2018. doi:10.1016/j.matpr.2017.12.364

[2] S. D. Desai, G. Megha, B. Avinash, K. Sudhanva, S. Rasiya, K. Linganagouda. "Detection of microcalcification in digital mammograms by improved-MMGW segmentation algorithm", Proceedings - 2013 International Conference on Cloud and Ubiquitous Computing and Emerging Technologies, CUBE 2013, pp. 213–218, 2013. doi:10.1109/CUBE.2013.47

[3] P. Henrot, A. Leroux, C. Barlier, P. Genin. "Breast microcalcifications: The lesions in anatomical pathology", Diagnostic and Interventional Imaging, vol. 95, no. 2, pp. 141–152, 2014. doi:10.1016/j.diii.2013.12.011

[4] A. Redman, S. Lowes, A. Leaver. "Imaging techniques in breast cancer", Surgery (United Kingdom), vol. 34, no. 1, pp. 8–18, 2015. doi: 10.1016/j.mpsur.2015.10.004

[5] T. Balakumaran, I. Vennila, C. Shankar. "Detection of Microcalcification in Mammograms Using Wavelet Transform and Fuzzy Shell Clustering", International Journal of Computer Science and Information Security, vol. 7, no. 1, pp. 121–125, 2010

[6] J. Dheeba, S. T. Selvi. "A swarm optimized neural network system for classification of microcalcification in mammograms", Journal of Medical Systems, vol. 36, no. 5, pp. 3051–3061, 2012. doi:10.1007/s10916-011-9781-3

[7] T. Balakumaran, I. L. A. Vennila, C. G. Shankar. "Microcalcification Detection in Digital Mammograms using Novel Filter", Procedia Computer Science, vol. 2, pp. 272–282, 2010. doi:10.1016/j.procs.2010.11.035

[8] M. Goudarzi, K. Maghooli. "Extraction of fuzzy rules at different concept levels related to image features of mammography for diagnosis of breast cancer", Biocybernetics and Biomedical Engineering, vol. 38, no. 4, pp. 1004–1014, 2018. doi:10.1016/j.bbe.2018.09.002

[9] E. Catanzariti, G. Forni, A. Lauria, R. Prevete, M. Santoro. "A CAD System for the Detection of Mammographyc Microcalcifications Based on Gabor Transform", IEEE Symposium Conference Record Nuclear Science 2004., vol. 6, no. C, pp. 3599–3603, 2004. doi:10.1109/NSSMIC.2004.1466662

[10] M. A. Duarte, A. V. Alvarenga, C. M. Azevedo, A. F. C. Infantosi, W. C. A. Pereira. "Automatic microcalcifications segmentation procedure based on Otsu's method and morphological filters", Pan American Health Care Exchanges, PAHCE 2011 - Conference, Workshops, and Exhibits. Cooperation / Linkages: An Independent

Forum for Patient Care and Technology Support, pp. 102–106, 2011. doi:10.1109/PAHCE.2011.5871858

[11] S. S. Yasiran, A. K. Jumaat, A. Abdul Malek, F. H. Hashim, N. Dhaniah Nasrir, S. N. Azirah Sayed Hassan, N. Ahmad, R. Mahmud. "Microcalcifications segmentation using three edge detection techniques", 2012 IEEE International Conference on Electronics Design, Systems and Applications (ICEDSA), pp. 207–211, 2012. doi:10.1109/ICEDSA.2012.6507798

[12] P. Kuş, I. Karagöz. "Detection of microcalcification clusters in digitized X-ray mammograms using unsharp masking and image statistics", Turkish Journal of Electrical Engineering and Computer Sciences, vol. 21, no. SUPPL. 1, pp. 2048–2061, 2013. doi:10.3906/elk-1202-114

[13] Z. Chen, H. Strange, A. Oliver, E. R. E. Denton, C. Boggis, R. Zwiggelaar. "Topological Modeling and Classification of Mammographic Microcalcification Clusters", IEEE Transactions on Biomedical Engineering, vol. 62, no. 4, pp. 1203–1214, 2015. doi:10.1109/TBME.2014.2385102

[14] L. Civcik, B. Yilmaz, Y. Özbay, G. D. Emlik. "Detection of microcalcification in digitized mammograms with multistable cellular neural networks using a new image enhancement method: Automated lesion intensity enhancer (ALIE)", Turkish Journal of Electrical Engineering and Computer Sciences, vol. 23, no. 3, pp. 853–872, 2015. doi:10.3906/elk-1303-139

[15] S. Anand, S. Gayathri. "Mammogram image enhancement by two-stage adaptive histogram equalization", Optik, vol. 126, no. 21, pp. 3150–3152, 2015. doi:10.1016/j.ijleo.2015.07.069

[16] A. H. H. Alasadi, A. K. H. Al-saedi. "A Method for Microcalcifications Detection in Breast Mammograms", Journal of Medical Systems, vol. 41, no. 68, pp. 1–9, 2017. doi:10.1007/s10916-017-0714-7

[17] Y. Guo, M. Dong, Z. Yang, X. Gao, K. Wang, C. Luo, Y. Ma, J. Zhang. "A new method of detecting micro-calcification clusters in mammograms using contourlet transform and non-linking simplified PCNN", Computer Methods and Programs in Biomedicine, vol. 0, no. 222, pp. 31–45, 2016. doi: 10.1016/j.cmpb.2016.02.019

[18] A. Abubaker. "An Adaptive CAD System to Detect Microcalcification in Compressed Mammogram Images", International Journal of Advanced Computer Science and Applications, vol. 8, no. 6, pp. 133–138, 2017. doi:10.14569/IJACSA.2017.080617

[19] B. Singh, M. Kaur. "An Approach for Enhancement of Microcalcifications in Mammograms", Journal of Medical and Biological Engineering, vol. 37, no. 4, pp. 567–579, 2017. doi:10.1007/s40846-017-0276-7

[20] V. Bhateja, M. Misra, S. Urooj. "Human visual system based unsharp masking for enhancement of mammographic images", Journal of Computational Science, vol. 21, pp. 387–393, 2017. doi:10.1016/j.jocs.2016.07.015

[21] D. Meersman, P. Scheunders, D. Van Dyck. "Detetction of Microcalcifications Using Non-linear Filtering", 9th European Signal Processing Conference, Rhodes, 1–4

[22] M. Heath, K. Bowyer, D. Kopans, R. Moore, W. P. Kegelmeyer. "The Digital Database for Screening Mammography", M. J. Yaffe (Ed.), Proceedings of the Fifth International Workshop on Digital Mammography, Medical Physics Publishing, 212–218

[23] A. Aydın Yurdusev. "The Data", from https://aysehoca.wordpress.com/the-data/

[24] M. A. Duarte, A. V Alvarenga, C. M. Azevedo, M. Julia, G. Calas, A. F. C. Infantosi, W. C. A. Pereira. "Evaluating geodesic active contours in microcalcifications segmentation on mammograms", Computer Methods and Programs in Biomedicine, vol. 122, no. 3, pp. 304–315, 2015. doi:10.1016/j.cmpb.2015.08.016

[25] P. Shi, J. Zhong, A. Rampun, H. Wang. "A hierarchical pipeline for breast boundary segmentation and calcification detection in mammograms", Computers in Biology and Medicine, vol. 96, no. March, pp. 178–188, 2018. doi:10.1016/j.compbiomed.2018.03.011

[26] J. R. Movellan. "Tutorial on Gabor Filters", University of California San Diago Open Source Document, 1–23

[27] J. G. Daugman. "Uncertainty relation for resolution in space, spatial frequency, and orientation optimized by two-dimensional visual cortical filters", Optical Society of America, vol. 2, no. 7, pp. 1160–1169, 1985. doi: 10.1364/JOSAA.2.001160

[28] N. Petkov, P. Kruizinga. "Biological Cybernetics Computational models of visual neurons specialised in the detection of periodic and aperiodic oriented visual stimuli : bar and grating cells", Biological Cybernetics, vol. 76, pp. 83–96, 1997. doi: 10.1007/s004220050323

[29] P. Kruizinga, N. Petkov. "Nonlinear Operator for Blob Texture Segmentation", IEEE Transactions on Image Processing, vol. 8, no. 1, pp. 881–885, 1999 http://hdl.handle.net/11370/fdc1250f-1063-4628-bc7a-13b0135f6213.

[30] B. Kamgar-Parsi, B. Kamgar-Parsi, A. Rosenfeld. "Optimum Laplacian for Digital Image Processing", International Conference on Image Processing, pp. 0–3, 1997. doi:10.1109/ICIP.1997.638599

[31] S. Shaikh, A. Choudhry, R. Wadhwani. "Analysis of Digital Image Filters in Frequency Domain", International Journal of Computer Applications. vol. 140, no. 6, pp. 12–19, 2016. doi: 10.5120/ijca2016909330

[32] S. Halkiotis, T. Botsis, M. Rangoussi. "Automatic detection of clustered microcalcifications in digital mammograms using mathematical morphology and neural networks", Signal Processing, vol. 87, no. 7, pp. 1559–1568, 2007. doi:10.1016/j.sigpro.2007.01.004

[33] H. S. Sheshadri, A. Kandaswamy. "Experimental investigation on breast tissue classification based on statistical feature extraction of mammograms", Computerized Medical Imaging and Graphics, vol. 31, no. 1, pp. 46–48, 2007. doi:10.1016/j.compmedimag.2006.09.015

[34] I. D. Borlea, R. E. Precup, F. Dragan, A. B. Borlea. "Centroid update approach to K-means clustering", Advances in Electrical and Computer Engineering, vol. 17, no. 4, pp. 3–10, 2017. doi:10.4316/AECE.2017.04001

[35] S. Chakraborty, S. Das. "K−Means clustering with a new divergence-based distance metric: Convergence and performance analysis", Pattern Recognition Letters, vol. 100, pp. 67–73, 2017. doi:10.1016/j.patrec.2017.09.025

[36] T. Zhang, F. Ma. "Improved rough k-means clustering algorithm based on weighted distance measure with Gaussian function", International Journal of Computer Mathematics, vol. 94, no. 4, pp. 663–675, 2017. doi:10.1080/00207160.2015.1124099

[37] R. Zall, M. R. Kangavari. "On the Construction of Multi-Relational Classifier Based on Canonical Correlation Analysis", International Journal of Artificial Intelligence, vol. 17, no. 2, pp. 23–43, 2019

[38] D. Saraswathi, E. Srinivasan. "Performance Analysis of Mammogram CAD System Using SVM and KNN Classifier", International Conference on Inventive Systems and Control, IEEE, Coimbatore, India, 1–5. doi: 10.1109/ICISC.2017.8068653

[39] J. Ren. "ANN vs. SVM: Which one performs better in classification of MCCs in mammogram imaging", Knowledge-Based Systems, vol. 26, pp. 144–153, 2012. doi:10.1016/j.knosys.2011.07.016

[40] E. D. Übeyli, I. Güler. "Multilayer perceptron neural networks to compute quasistatic parameters of asymmetric coplanar waveguides", Neurocomputing, vol. 62, nos. 1–4, pp. 349–365, 2004. doi:10.1016/j.neucom.2004.04.005

[41] İ. Dalkıran, K. Danışman. "Artificial neural network based chaotic generator for cryptology", Turk J Elec Eng & Comp Sci, vol. 18, no. 2, pp. 225–240, 2010. doi:10.3906/elk-0907-140

[42] N. Panahi, M. G. Shayesteh, S. Mihandoost, B. Zali Varghahan. "Recognition of different datasets using PCA, LDA, and various classifiers", 2011 5th International Conference on Application of Information and Communication Technologies, AICT 2011, 2011. doi:10.1109/ICAICT.2011.6110912

[43] A. K. Junoh, M. N. Mansor. "Safety System Based on Linear Discriminant Analysis", International Symposium on Instrumentation & Measurement, Sensor Network and Automation (IMSNA), pp. 32–34, 2012. doi: 10.1109/MSNA.2012.6324510

[44] P. N. Belhumeur, J. P. Hespanha, D. J. Kriegman. "Eigenfaces vs. fisherfaces: Recognition using class specific linear projection", IEEE Transactions on Pattern Analysis and Machine Intelligence, vol. 19, no. 7, pp. 711–720, 1997. doi:10.1109/34.598228

[45] H. Yu, J. Yang. "A direct LDA algorithm for high-dimensional data - with application to face recognition", Pattern Recognition, vol. 34, no. 10, pp. 2067–2070, 2002. doi:10.1016/s0031-3203(00)00162-x

[46] M. Saddique, K. Asghar, U. I. Bajwa, M. Hussain, Z. Habib. "Spatial Video Forgery Detection and Localization using Texture Analysis of Consecutive Frames", Advances in Electrical and Computer Engineering, vol. 19, no. 3, pp. 97–108, 2019. doi:10.4316/AECE.2019.03012

[47] M. Hekim. "The classification of EEG signals using discretization-based entropy and the adaptive neuro-fuzzy inference system", Turkish Journal of Electrical Engineering and Computer Sciences, vol. 24, no. 1, pp. 285–297, 2016. doi:10.3906/elk-1306-164